Vibrational Spectroscopic Study on the Solid-State Phase Transition of Poly(oxymethylene) Single Crystals from the Orthorhombic to the Trigonal Phase

Masamichi Kobayashi* and Hirofumi Morishita†

Department of Macromolecular Science, Faculty of Science, Osaka University, Toyonaka, Osaka 560, Japan

Masaki Shimomura and Masatoshi Iguchi

Research Institute for Polymers and Textiles, Yatabehigashi, Tsukuba, Ibaraki 305, Japan.
Received December 11, 1986

ABSTRACT: The thermally induced solid-state phase transition of poly(oxymethylene) from the orthorhombic to the trigonal phase has been investigated on micron-sized single crystals by means of DSC and Raman microspectroscopic methods. On heating, the metastable orthorhombic single crystals transform irreversibly to the stable trigonal form at 69 °C with an endotherm of 0.6 kJ/mol per OCH_2 unit, indicating that instability of the orthorhombic phase is not responsible for the cohesive energy but for its low entropy term compared with that of the trigonal phase. The higher entropy term in the trigonal phase may be attributed to the onset of a rotational fluctuation around the chain axis of the 9/5 helix, which is cylindrically more symmetric and of smaller moment of inertia than the 2/1 helix of the orthorhombic phase. This is supported by the fact that with rising temperature the far-infrared band due to the rotatory lattice vibration smears appreciably in the trigonal phase. The morphology, the fiber axis orientation, and the extended-chain structure of the starting orthorhombic crystals remain unchanged throughout the transition. On a plate-shaped single crystal of trigonal poly(oxymethylene), polarized Raman spectra have been taken by the microprobe technique. Two E_1 Raman bands have been found to exhibit a distinct longitudinal optic–transverse optic splitting of 10–12 cm^{-1}.

Introduction

By ordinary melt or solution crystallization, poly(oxymethylene), $(CH_2O)_n$ (abbreviated as POM), is obtained in a trigonal modification consisting of 9/5[1] or 29/16[2] helical molecules. Two decades ago Carazzolo and Putti succeeded in preparing another crystal modification that belonged to an orthorhombic system consisting of 2/1 helical molecules.[3] The structure of orthorhombic POM (o-POM) has been investigated by means of X-ray diffraction,[4] infrared absorption,[5,6] and Raman scattering.[7,8]

The orthorhombic modification has been recognized as a metastable phase. It transforms immediately to the stable trigonal phase when the sample is heated above 70 °C or is subjected to mechanical deformation (by stretching, rolling, or pressing). The solid-state phase transition of POM is accompanied by changes in molecular conformation (from the 2/1 to the 9/5 helix) and in molecular packing (from the orthorhombic to hexagonal). Elucidation of the molecular mechanism of this phase transition seems to be of fundamental importance in order to understand the structure–property relationship of solid POM. Until now, however, details of its thermodynamic and structural features, even the basic thermogram, remain unclarified.

Previous structural studies of o-POM have been done on powder samples because any orientation process induces the phase transition. Recently, we found that o-POM may be obtained in a micron-sized single-crystal form having a specific shape resembling a "moth".[9] Orientation of the crystallographic axes in the single crystal was investigated by polarized Raman microspectroscopy,[10] infrared microspectroscopy,[11] and normal-mode analysis.[10] In addition, one of the present authors (M.I.) succeeded in preparing high-purity samples of o-POM crystals having a different morphology.[12]

With these o-POM samples we have investigated, in the present work, the thermogram (by DSC) and the morphological as well as orientational changes (by polarized Raman microspectroscopy) that take place during the solid-state phase transition. The origin of the thermodynamic stability of the trigonal phase is considered from the spectroscopic viewpoint.

In the course of this work we obtained moth-shaped single crystals of t-POM by thermal phase transition of o-POM crystals of the same shape. With this sample we were able to measure for the first time the polarized Raman spectra of t-POM by means of the microprobe technique. The results are compared with the previously obtained polarized infrared[13] and unpolarized Raman spectra.[10,14] Our interest is focused on observing the LO–TO splitting anticipated for the Raman-active polar phonons (the E_1 species), being characteristic of the piezoelectric space group $P3_1$-C_3^2 of t-POM.

Experimental Section

(1) Samples. Moth-shaped single crystals of o-POM were found in the sample obtained in a special batch which had originally been designed to prepare needlelike single crystals (polymer whiskers) of t-POM by a cationic polymerization of trioxane.[9] In the optical micrograph of this sample we observed moth-shaped crystals of o-POM with dimensions as large as 30–50-μm diameter and about 2-μm thickness mixed with needlelike crystals of t-POM (Figure 1). They were subjected to the microfocus Raman measurement without separation from the needlelike crystals. On the surface of the mothlike crystals there are observed parallel striations. We define the sample-based Cartesian coordinates as follows: X is parallel to the striation, Y perpendicular to it within the plate surface, and Z normal to the plate surface. The directions X, Y, and Z have been found to be parallel respectively to the c, a, and b axes of the orthorhomic unit cell.[10,11] The high-purity o-POM sample was supplied from Research Institute for Polymers and Textiles.[12] Morphologically, this sample consists of spherical particles, each comprising a number of rodlike crystalline units packed at random, the crystallographic c axis being parallel to the long axis. This sample was used for the DSC and IR measurements.

(2) Microfocus Raman Measurement. Details of the instrument used are described in ref 10. This consists of an epi-illumination optical microscope (Olympus BH-2) and a JASCO CT-1000D double monochromator with a 1-m focal length,

† Present address: Faculty of Education, Nagasaki University, Nagasaki-City, Nagasaki 852, Japan.

0024-9297/87/2220-2453$01.50/0

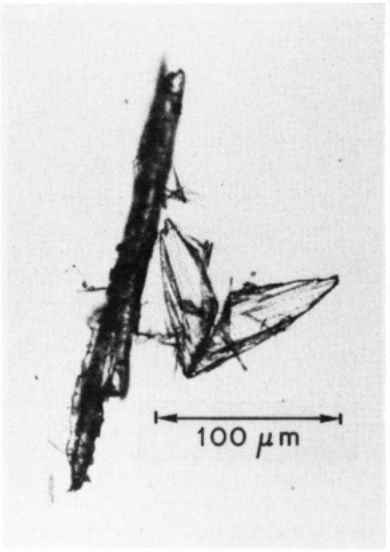

Figure 1. Optical micrograph of a moth-shaped o-POM single crystal mixed with needlelike crystals of t-POM.

equipped with a system for polarization measurement. The powder sample of needlelike crystals containing mothlike crystals was dispersed with a small amount of water on a glass plate. A mothlike crystal having a clear optical surface was selected in the microscope field of view, and the laser beam (the 514.5-nm light from an Ar^+ laser) polarized in the X or Y direction was focused at a selected position on the surface through the objective of the microscope. The backward scattered light was collected by the same objective and guided into a monochromator through an analyzer for the polarization measurement. With three scattering geometries, $Z(XX)\bar{Z}$, $Z(YY)\bar{Z}$, and $Z(XY)\bar{Z}$ (according to the Porto notation), the polarized spectra were recorded.

Phase Transition from the Orthorhombic to the Trigonal Form

(1) Thermal Behavior. In the DSC thermogram (on heating) of the high-purity sample of o-POM reported in ref 12, there are no distinct sharp peaks except for the strongest endothermic peak at 190 °C corresponding to the melting of the resultant trigonal phase. In the vicinity of the transition temperature, which was believed to be located in the range of 75–80 °C from the change in the X-ray diffraction pattern, there appear diffuse multiple peaks. In our experiment, done at an early stage, we obtained a similar result. In that case, as usual, the sample was put in a pan, pressed with a cover plate, and then subjected to the measurement. Considering that the appearance of diffuse multiple peaks could be caused by a partial transformation induced by a mechanical deformation that might take place during the pressing process, we prepared the DSC sample without pressing. Then, as shown in Figure 2, a sharp endothermic peak appeared at 69 °C with ΔH = 0.6 kJ/mol per OCH_2 unit before the melting peak of t-POM at 187 °C. The melting point of the resultant t-POM is similar to those of needlelike crystals and significantly higher than those of typical melt-crystallized samples (ca. 175 °C). The appearance of the endothermic peak of the o → t phase transition indicates that the instability of the orthorhombic phase is not responsible for the enthalpy term but for the entropy term. This is consistent with the fact that the crystal density of o-POM (ρ_c = 1.54 g/cm^3) is 3% higher than that of t-POM (ρ_c = 1.49 g/cm^3). Therefore, o-POM has higher cohesive energy, being energetically more stable, than t-POM. The higher entropy of t-POM seems to be caused by the rotational fluctuation around the chain axis of the 9/5 helix, which is cylindrically more symmetric and has

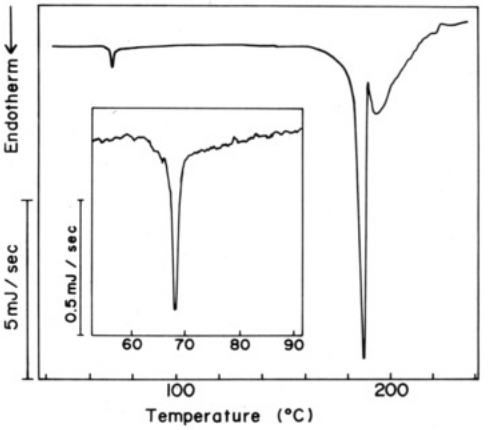

Figure 2. Differential scanning calorimetry curve of o-POM (apparatus, Seiko DSC-20; heating rate, 2 °C/min; sample weight, 3.0 mg).

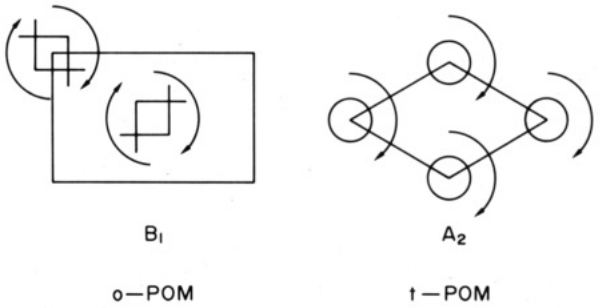

Figure 3. Infrared-active rotatory lattice mode of o-POM and t-POM.

smaller moment of inertia than the 2/1 helix of o-POM. This is reflected in the far-infrared band due to the lattice mode (Figure 3) of the two crystalline phases. In o-POM, the in-phase rotatory mode $R_c(B_1)$ appears as a sharp band at 128 cm^{-1} at room temperature and shifts to 142 cm^{-1} at 93 K (Figure 4, top). On the other hand, the corresponding mode $R_c(A_2)$ of t-POM (taken on needlelike crystals) appears at 101 cm^{-1} as a weak but distinct band at 102 K and almost smears into the background at room temperature (Figure 4, bottom). The smearing of the band in t-POM may be related to a dephasing of the mode caused by the rotational fluctuation.

(2) Morphological Change. A change in the morphological structure of single crystals during the thermal phase transition from o-POM to t-POM was investigated by the polarized microscope and microfocus Raman spectroscopy on both the rodlike and moth-shaped crystals. It was found that the shape as well as the orientation of the fiber axis remained unchanged throughout the transition. The phase transition was followed also by the change in the infrared spectrum (Figure 5). The infrared spectrum of the resultant t-POM crystal is similar to that of needlelike crystals rather than that of melt-crystallized samples. For example, the $A_2(4)$ and the $A_2(5)$ modes appear, respectively, at 895 and 220 cm^{-1} (characteristic positions of the needlelike crystal of t-POM), instead of 903 and 235 cm^{-1} of the melt-crystallized sample.[13,15] This indicates that the resultant trigonal phase consists of fully extended chains, being consistent with its high melting point mentioned in the preceding subsection.

Microfocus Raman Spectra of t-POM Single Crystals

By the thermal phase transition of the moth-shaped single crystals of o-POM, we obtained the t-POM single crystals having the same habit. On this sample we are able

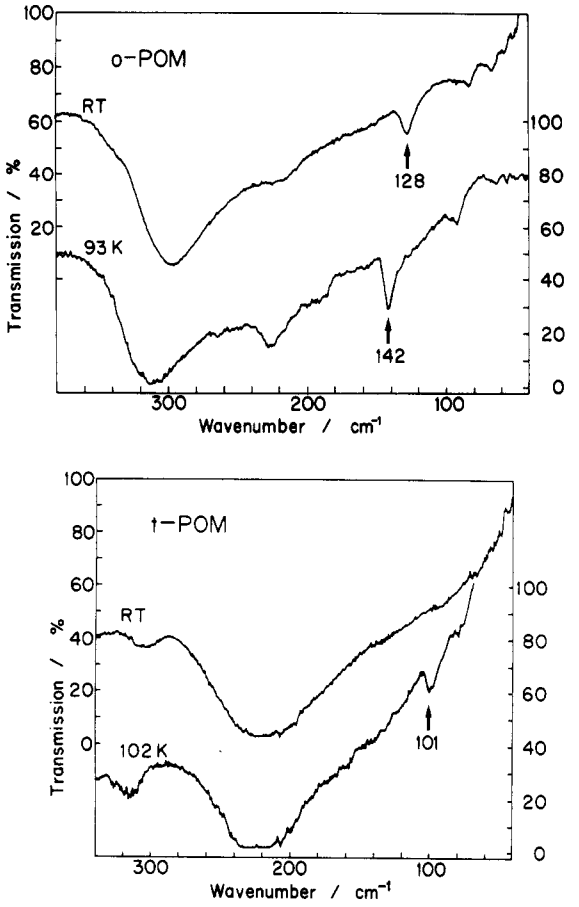

Figure 4. Far-infrared spectra of two modifications of poly(oxymethylene) measured at room and lowered temperatures: (top) o-POM (rodlike crystals); (bottom) t-POM (needlelike whiskers).

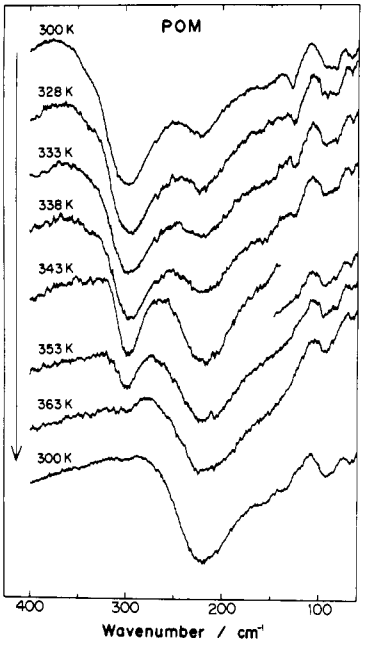

Figure 5. Far-infrared spectral change on the thermal transformation from the orthorhombic to trigonal phase.

to take, for the first time, the polarized Raman spectra using the microprobe technique. In Figure 6 the spectra are compared with those of the o-POM crystal.

It should be mentioned here the polarization scrambling in the Raman microprobe experiment. As described in ref 10 and 16, use of a sharp focusing objective, which acts as the condenser and as the collection lens, causes spurious

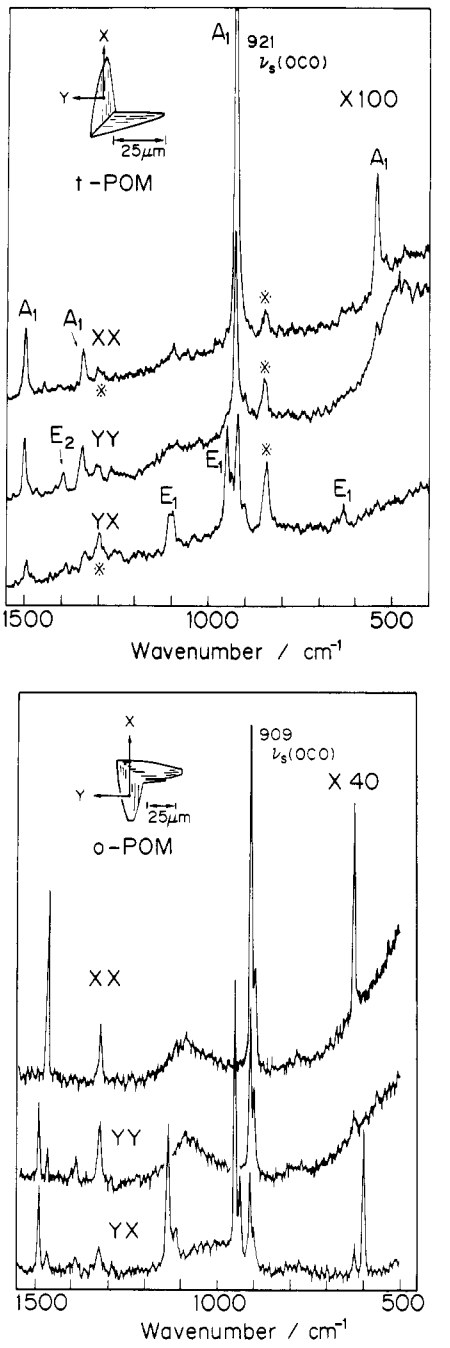

Figure 6. Polarized microfocus Raman spectra of two modifications of poly(oxymethylene) taken on moth-shaped crystals of (top) t-POM and (bottom) o-POM. The asterisk denote ghost peaks.

polarizations in both the incident and scattered lights. Mixing of the polarization component along the depth direction (the Z direction in the present case) is substantial, while that within the focal plane (the XY plane) is negligible. The degree of polarization scrambling depends on the magnification, or more precisely, on the numerical aperture NA, of the objective used: the degree of mixing is more the higher is the NA value. Insertion of an aperture or an iris diaphragm in front of the telemeter lens reduces the effective NA value and, therefore, diminishes the mixing effect. On the other hand, the light collection power is higher for the objective having higher magnification (or NA value). Therefore, it is necessary to select the optimal NA value, depending on the sample conditions.

The variation in the relative band intensities with a change in the magnification of the objective and also with the aperture insertion has been discussed in ref 10 for the

Table I
Number of Normal Modes (n) and Infrared and Raman Polarization of the t-POM Molecule

species	n	infrared	Raman
A_1	5	forbidden	$(\alpha_{aa} + \alpha_{a^*a^*}), \alpha_{cc}$
A_2	5	μ_c	forbidden
E_1	11 × 2	(μ_a, μ_{a^*})	$(\alpha_{ac}, \alpha_{a^*c})$
E_2	12 × 2	forbidden	$(\alpha_{aa} - \alpha_{a^*a^*}, \alpha_{aa^*})$
E_3	12 × 2	forbidden	forbidden
E_4	12 × 2	forbidden	forbidden

case of o-POM single crystal. In the present case, we used five objectives of magnifications ×100, ×50, ×40, ×20, and ×10 with various apertures of different diameters. The bottom part of Figure 6 was taken with a ×40 objective without aperture and the top part of Figure 6 with a ×100 objective with an aperture of 2-mm diameter. Although both spectra contain weak bands resulting from polarization mixing, they are not serious for the following discussion concerning molecular orientation.

The zone-center normal modes of the 9/5 helical molecule of t-POM are classified into six irreducible representations as listed in Table I. In this table, c and a mean the crystallographic axes of the trigonal lattice and a^* the direction perpendicular to the ac plane. The strong bands in the (XX) spectrum (at 1499, 1344, 921, and 542 cm^{-1}) are assigned to the A_1 modes on the basis of the previous result of the vibrational analysis.[13] Except for the 542-cm^{-1} band, they are observed also in the (YY) spectrum. The 1395-cm^{-1} band, which is the only E_2 mode detectable at room temperature,[14] appears in the (YY) polarization. In the (XY) spectrum the E_1 bands appear around 1095, 940, and 636 cm^{-1}. Comparing this with the predicted Raman polarization given in Table I, we conclude that the c axis is parallel to X as in the starting o-POM single crystal.

It should be noted that the E_1 bands around 1095 and 940 cm^{-1} are split into a doublet. The t-POM unit cell belongs to a polar space group $P3_1$-C_3^2 (or $P3_2$-C_3^3), containing one 9/5 helix. Among the zone-center molecular modes, only those belonging to the E_1 species are active in both infrared and Raman spectra (the Raman-active polar phonons). Therefore, we are able to anticipate, at least in principle, that the E_1 Raman bands give rise to an angular dispersion (i.e., variation in the band position with a change in the angle between the wavenumber vector $\mathbf{q}$ and the mode polarization) or the band splitting into the LO (longitudinal optic) and TO (transverse optic) modes. As illustrated in Figure 7, when the c axis is located perpendicular to the wavenumber vector $\mathbf{q} = \mathbf{q}_i - \mathbf{q}_s$ ($\mathbf{q}_i$ and $\mathbf{q}_s$ are the wavenumber vectors of the incident and scattered lights, respectively), both the LO and TO components of the doubly degenerate E_1 species are observed independently of the scattering angle (in both right-angle and backward scattering). In the present case the $E_1(7)$ mode appears at 1108 (LO) and 1098 (TO) cm^{-1} (with the band gap of $\Delta\nu = 10$ cm^{-1}) and the $E_1(8)$ mode at 952 (LO) and 940 (TO) cm^{-1} ($\Delta\nu = 12$ cm^{-1}). The frequencies of the TO components agree with the peak positions of the infrared bands.

The magnitude of the LO–TO splitting should be approximately proportional to the infrared intensity and inversely proportional to the mode frequency.[17-19] The $E_1(7)$ and $E_1(8)$ modes for which distinct LO–TO splittings are observed give rise to very strong infrared intensities. For the $E_1(9)$ mode showing a medium-intense absorption, we expect to detect an LO–TO splitting, although the observed Raman profile has only one peak at 636 cm^{-1}.

The Raman LO–TO splitting characteristic of polar crystals has been studied extensively in some ionic crystals

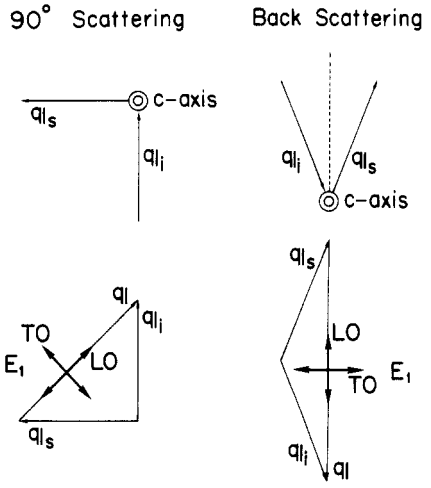

Figure 7. Raman scattering geometries and the LO and TO modes to be measured for the doubly degenerate E_1 species. The incident and scattered photon propagation vectors are denoted by $\mathbf{q}_i$ and $\mathbf{q}_s$, respectively, and the phonon propagation vector by $\mathbf{q} = \mathbf{q}_i - \mathbf{q}_s$.

such as quartz,[19,20] $BaTiO_3$,[21] etc. On the other hand, only limited examples are known for molecular solids. In previous papers[22-24] one of the present authors (M.K.) and his co-workers studied the angular and the polariton dispersion of the polar crystal of trioxane, a cyclic trimer of oxymethylene. The magnitudes of LO–TO splitting of the E modes, corresponding to the $E_1(7)$ and $E_1(8)$ modes of t-POM, are 19.9 and 9.2 cm^{-1}, respectively. As for crystalline polymers, LO–TO splitting of 1–6 cm^{-1} has been observed for the Raman bands of poly(vinylidene fluoride) form I (piezoelectric phase).[25]

Registry No. POM, 9002-81-7.

References and Notes

(1) Tadokoro, H.; Yasumoto, T.; Murahashi, S.; Nitta, I. *J. Polym. Sci.* **1960**, *44*, 266. Uchida, T.; Tadokoro, H. *J. Polym. Sci., Polym. Phys. Ed.* **1967**, *5*, 63.
(2) Carazzolo, G. A. *J. Polym. Sci., Part A* **1963**, *1*, 1573.
(3) Carazzolo, G. A.; Putti, G. *Chim. Ind. (Milan)* **1963**, *45*, 771.
(4) Carazzolo, G. A.; Mammi, M. *J. Polym. Sci., Part A* **1963**, *1*, 965.
(5) Zamboni, V.; Zerbi, G. *J. Polym. Sci., Part C* **1964**, *7*, 153.
(6) Zerbi, G.; Masetti, G. *J. Mol. Spectrosc.* **1967**, *22*, 284.
(7) Zerbi, G.; Hendra, P. J. *J. Mol. Spectrosc.* **1968**, *27*, 17.
(8) Boerio, F. J.; Cornell, D. D. *J. Chem. Phys.* **1972**, *56*, 1516.
(9) Kobayashi, M.; Itoh, Y.; Tadokoro, H.; Shimomura, M.; Iguchi, M. *Polym. Commun.* **1983**, *24*, 38.
(10) Kobayashi, M.; Morishita, H.; Ishioka, T.; Iguchi, M.; Shimomura, M.; Ikeda, T. *J. Mol. Struct.* **1986**, *146*, 155.
(11) Morishita, H.; Kobayashi, M. *Rep. Progr. Polym. Phys. Jpn.*, in press.
(12) Iguchi, M. *Polymer* **1983**, *24*, 915.
(13) Tadokoro, H.; Kobayashi, M.; Kawaguchi, Y.; Kobayashi, A.; Murahashi, S. *J. Chem. Phys.* **1963**, *38*, 703.
(14) Sugeta, H.; Miyazawa, T.; Kajiura, T. *J. Polym. Sci., Polym. Lett.* **1969**, *7*, 251.
(15) Shimomura, M.; Iguchi, M. *Polymer* **1982**, *23*, 509.
(16) Bremard, C.; Dhamellincourt, P.; Larreyns, J.; Turrel, G. *Appl. Spectrosc.* **1985**, *39*, 1036.
(17) Born, M.; Huang, K. *Dynamical Theory of Crystal Lattices*; Clarendon: Oxford, 1954.
(18) Hayes, W.; Loudon, R. *Scattering of Light by Crystals*; Wiley: New York, 1978.
(19) Shapiro, S. M.; Axe, J. D. *Phys. Rev. B* **1972**, *6*, 2420.
(20) Elcombe, M. M. *Proc. Phys. Soc.* **1967**, *91*, 947.
(21) DiDomenico, M., Jr.; Wempel, S. H.; Porto, S. P. S. *Phys. Rev.* **1968**, *174*, 522.
(22) Kobayashi, M. *J. Chem. Phys.* **1982**, *76*, 1187.
(23) Kobayashi, M.; Furumi, K. *J. Chem. Phys.* **1982**, *76*, 4725.
(24) Kobayashi, M.; Tashiro, K.; Yagi, N. *Jpn. J. Appl. Phys.* **1985**, *24*, Suppl. 24-2, 500.
(25) Tashiro, K.; Itoh, Y.; Kobayashi, M.; Tadokoro, H. *Macromolecules* **1985**, *18*, 2600.